

Active Extrinsic Contact Sensing: Application to General Peg-in-Hole Insertion

Sangwoon Kim, Alberto Rodriguez

Abstract—We propose a method that actively estimates the location of contact between a grasped rigid object and its environment, and uses this as input to a peg-in-hole insertion policy. An estimation model and an active tactile feedback controller work collaboratively to get an accurate estimate of the external contacts. The controller helps the estimation model get a better estimate by regulating a consistent contact mode. The better estimation makes it easier for the controller to regulate the contact. To utilize this contact estimate, we train an object-agnostic insertion policy that learns to make use of the series of contact estimates to guide the insertion. In contrast with previous works that learn a policy directly from tactile signals, since this policy is in contact configuration space, can be learned directly in simulation. Lastly, we demonstrate and evaluate the active extrinsic contact line estimation and the trained insertion policy together in a real experiment. We show that the proposed method inserts various-shaped test objects with higher success rates and fewer insertion attempts than previous work with end-to-end approaches. See supplementary video and results at <https://sites.google.com/view/active-extrinsic-contact>.

I. INTRODUCTION

The ability to sense and utilize tactile feedback between fingers and grasped object is a key foundation to dexterous manipulation skills [1]. Tactile sensing can be used as a feedback signal to regulate desired contact configurations [2]. One major problem in tactile feedback control is localizing and controlling an external contact: a contact between the grasped object and its environment. For example, consider pivoting an unknown object resting on a surface while avoiding slip at the contact between the object and the surface. It requires an ability to regulate the external contact using indirect observations, possibly through tactile sensing.

In the peg-in-hole insertion task, the external contact matters. A misalignment between the peg and the hole results in contact during the insertion attempt. The contact triggers a tactile signal, which can be used to localize the contact or plan the next insertion attempt. Key challenges in this task are as follows:

- The tactile signal is a partial observation of the contact state; many different contact configurations can cause the same tactile signal [3].
- The frictional contact mechanics that govern the alignment and insertion dynamics are sensitive to switching contact modes.

This research is supported by the HKSAR Innovation and Technology Fund (ITF) ITS-104-19F, and by the Mitsubishi Electric Research Laboratory (MERL).

Sangwoon Kim and Alberto Rodriguez are with the Department of Mechanical Engineering, Massachusetts Institute of Technology, <sangwoon, albertor>@mit.edu

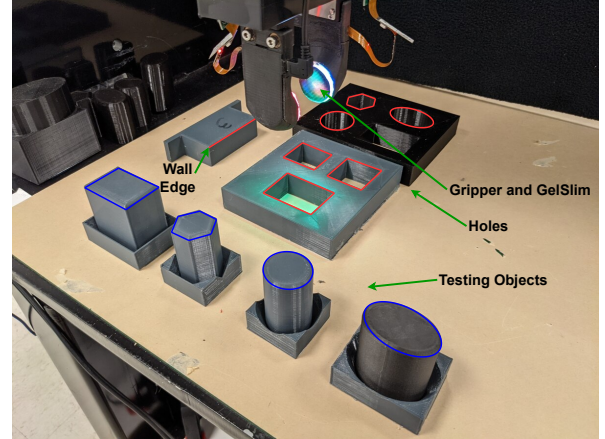


Fig. 1: Experimental setup: Gripper with GelSlim [5], different objects (blue), and different environments (red)

In this work, we tackle both the extrinsic contact localization problem and the peg-in-hole insertion task in a combined framework. For the extrinsic contact localization, we use a factor graph solved with incremental smoothing and mapping (iSAM) [4] to fuse the information of robot proprioception and tactile measurements. The factor graph works collaboratively with an active tactile feedback controller that attempts to pivot the object about a regulated external contact to generate sufficient observations to estimate the contact line between an unknown object and an unknown environment. The contact line estimation is then used as an input to the insertion policy, as opposed to the end-to-end approach where the policy takes directly as input the raw tactile feedback. Since the input to the policy is a low dimensional representation (a contact line), the policy training can be done in a simple simulation so there is no need to collect training data in a real experiment. Lastly, we demonstrate and evaluate the extrinsic contact line estimation and the trained insertion policy in a set of real experiments.

II. RELATED WORK

A. Tactile Sensing and Feedback

Prior work showed that tactile measurements can be used for state estimation. Bicchi, et al. [6] used force measurements to estimate a contact location when the force is directly exerted on the robot with known geometry. Yu and Rodriguez [7] combined force and visual sensing to estimate the pose of a known planar object in planar manipulation. They also used a similar framework to estimate the SE(3) pose of a known object that is in touch with an external environment [8].

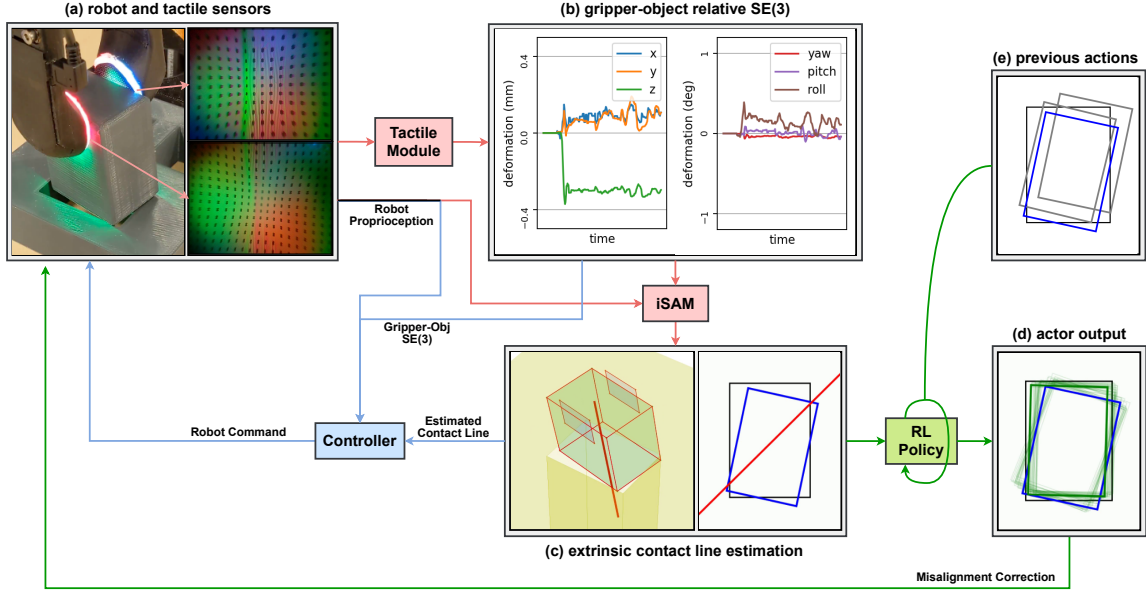


Fig. 2: Approach Overview. Estimation module (red) and active tactile feedback controller (blue) run collaboratively to estimate extrinsic contact line. RL policy (green) takes the estimated extrinsic contact line as input and computes the next action. (a) Insertion attempt and tactile images captured by GelSlim fingers. (b) Gripper-Object relative displacement computed by a learned tactile module. (c) 3D and top view of the extrinsic contact line estimation. The bold red line is the current estimate. (d) RL Actor output. The blue rectangle is the current pose and the green rectangles are the candidate poses for the next insertion attempt. (e) History of previous attempts that feed into the recurrent RL architecture.

The recent appearance of high-resolution vision-based tactile sensors like GelSight [9] and GelSlim [10], [5] enabled more accurate estimation. These sensors capture the physical interaction between the robot fingers and the grasped object as high-resolution images. Bauza, et al. [11], [12] used tactile images to map and localize the relative pose of a known grasped object. Ma, et al. [13] conducted inverse finite element method (iFEM) on tactile images to reconstruct a dense tactile force distribution. Sodhi, et al. [14] developed a factor graph model that finds a maximum a posteriori (MAP) estimate of an end-effector and an object pose in planar manipulation from only a vision-based tactile sensor [15] and robot proprioception. While the aforementioned work focused on estimating the states of an object or an interface that is in direct touch with a tactile sensor, Ma, et al. [16] focused on localizing extrinsic contacts: contact between a grasped object and an external environment. They accumulated a sequence of tactile images and used least-squares fitting [17] to estimate the location of the extrinsic contact point or line. All these estimation methods, however are passive, so they are limited to use the information they are presented with.

The tactile sensing and the state estimation can be used as a feedback signal to regulate the desired contact configuration. Dong, et al. [18] introduced a module that monitors incipient slip on the tactile sensor and used it to maintain a stable grasp. Hogan, et al. [19] developed a closed-loop tactile controller for dexterous manipulation primitives such as pulling, pivoting and pushing. They used a controller to maintain a sticking contact while executing the manipulation primitives. She, et al. [20] showed the use of tactile sensing for manipulating a cable. They learned a linear model for the cable sliding dynamics and implemented a linear quadratic

regulator (LQR) to keep the cable near the sensor center while sliding through the cable.

B. Peg-in-Hole Insertion

Early studies on peg-in-hole insertion relied on passive compliance of the gripper [21], which can be used when the object is chamfered and an initial misalignment is small. Other works assume a known object-hole model [22], [23]. These methods are object-specific and difficult to apply to unknown objects. More recently, model-free, end-to-end, learning-based approaches have been proposed [24], [25], [26], [27]. [24] used deep reinforcement learning (RL) for a high precision peg-in-hole task. They used a force/torque (F/T) sensor measurement and a robot position as input to a discrete action policy. [25] fused force and vision to address the peg-in-hole insertion task. [26] used supervised learning to map a raw tactile image sequence to a misalignment between peg and hole. However, since the tactile image is not a full observation of the state, their approach showed sub-optimal performance. The same group of researchers used end-to-end RL instead of supervised learning to overcome this limitation and showed an improvement in performance [27]. In these end-to-end (images-to-actions) approaches, simulating raw images is difficult so the training data was collected in real experiments.

III. METHODOLOGY

The task we solve is a typical peg-in-hole problem. We make several assumptions to implement our framework:

- Object bottom surfaces and hole top surfaces are flat.
- The misalignment between object and hole is an SE(2) displacement in the plane of contact.
- Objects and holes are un-chamfered.

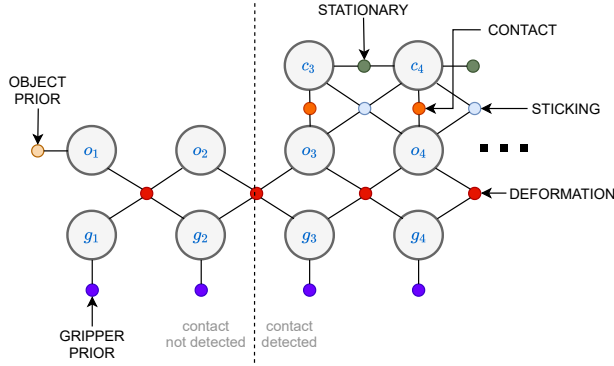


Fig. 3: Estimation factor graph

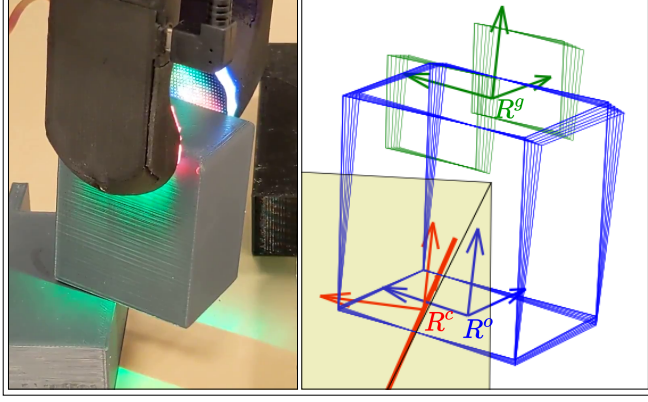


Fig. 4: Left: An object in contact with an edge. Right: Gripper (green) and object (blue) trajectories and an estimated contact line (red).

The approach is composed of two parts: the active extrinsic contact sensing and the insertion policy. In the active extrinsic contact sensing, an iSAM-based estimation graph works collaboratively with an active tactile feedback controller to estimate the extrinsic contact line. The controller helps the iSAM graph to improve the estimation by regulating a consistent extrinsic contact mode. The improved estimation from the iSAM graph helps the controller to better regulate the extrinsic contact. Then, the insertion policy, learned in simulation with reinforcement learning (RL), takes the estimated contact line as input and computes the next action for the insertion.

A. Tactile Module and iSAM Graph

We use GelSlim 3.0 [5], a vision-based tactile sensor, to capture the deformation image on the robot finger during the insertion (Fig.2a). The image is passed to a convolutional neural network (CNN) architecture, the tactile module, trained with supervised learning to estimate the relative SE(3) displacement between the gripper and the object due to the compliance of the finger (Fig.2b). The gripper-object relative displacement and the robot proprioception data are then used in the iSAM graph to infer the extrinsic contact line (Fig.2c).

Fig.3 shows the iSAM graph. Each color of small circles represents different types of factors. g_i , o_i , and c_i are the SE(3) gripper pose, object pose, and contact line as shown in Fig.4; xy surface of o_i represents the bottom surface of the

object and x -axis of c_i represents the estimated contact line. iSAM computes a maximum a posteriori (MAP) estimate for trajectories of the gripper pose G , the object pose O , and the contact line C , given the gripper pose measurements based on robot proprioception R , the gripper-object relative displacement D , and the initial object pose prior b_o :

$$G^*, O^*, C^* = \arg \max_{G, O, C} P(G, O, C, R, D, b_o) \quad (1)$$

Assuming Gaussian noise, solving for the MAP estimate becomes a nonlinear least-squares problem:

$$G^*, O^*, C^* = \arg \min_{G, O, C} \left\{ \sum_{t=1}^T \left\{ \|F_{gp}(g_t, r_t)\|_{\Sigma_{gp}}^2 + \|F_{def}(g_{t-1}, g_t, o_{t-1}, o_t, d_t)\|_{\Sigma_{def}}^2 + \|F_{ct}(o_t, c_t)\|_{\Sigma_{ct}}^2 + \|F_{tic}(o_{t-1}, o_t, c_{t-1}, c_t)\|_{\Sigma_{tic}}^2 + \|F_{stat}(c_{t-1}, c_t)\|_{\Sigma_{stat}}^2 + \|F_{op}(o_1, b_o)\|_{\Sigma_{op}}^2 \right\} \right\}, \quad (2)$$

where $F(\cdot)$ are cost functions for each factor. $\|\cdot\|_{\Sigma}$ is the Mahalanobis distance with covariance Σ . iSAM enables to add new measurements incrementally and update the estimation in real-time rather than solving it from scratch at every step.

Gripper prior (F_{gp}) and Object prior (F_{op}): We use unary factors to model the uncertainty of the gripper pose and initial object pose:

$$\|F_{gp}(g_t, r_t)\|_{\Sigma_{gp}}^2 := \|g_t \ominus r_t\|_{\Sigma_{gp}}^2 \quad (3)$$

$$\|F_{op}(o_1, b_o)\|_{\Sigma_{op}}^2 := \|o_1 \ominus b_o\|_{\Sigma_{op}}^2, \quad (4)$$

where r_t is the measured gripper pose based on robot proprioception and b_o is the prior knowledge about the initial object pose.

GelSlim deformation factor (F_{def}): Relative SE(3) displacement between gripper and object computed by the tactile module is incorporated as the GelSlim deformation factor:

$$\|F_{def}(g_{t-1}, g_t, o_{t-1}, o_t, d_t)\|_{\Sigma_{def}}^2 := \|((g_{t-1}^{-1} o_{t-1})^{-1} (g_t^{-1} o_t)) \ominus d_t\|_{\Sigma_{def}}^2, \quad (5)$$

where d_t is the change in the relative displacement from $t-1$ to t .

Contact factor (F_{ct}): To constrain the estimated contact line to lie on the object bottom surface, we use a binary factor:

$$\|F_{ct}(o_t, c_t)\|_{\Sigma_{ct}}^2 := \|(o_t^{-1} c_t)_{z^c, R_{xc}^c, R_{yc}^c}\|_{\Sigma_{ct}}^2, \quad (6)$$

where the subscript z^c, R_{xc}^c, R_{yc}^c indicates that we only constrain the components that move out of the object's bottom surface.

Sticking factor (F_{tic}): Fig.6 shows an example of an object touching an environment and tilting at a small angle. In such a case, it is difficult to infer the actual contact point with only geometric constraints. All the green points in the figure will seem to satisfy the geometric constraints for a certain object height. Therefore, while we can get a reasonable estimate in the horizontal direction, the estimated height of the contact will be uncertain. However, if we use a controller to regulate

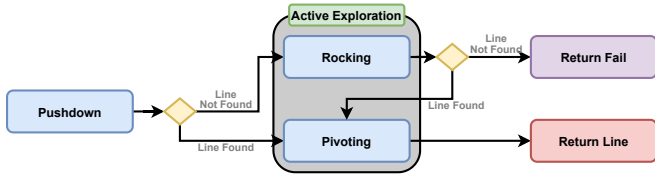


Fig. 5: Active tactile feedback controller

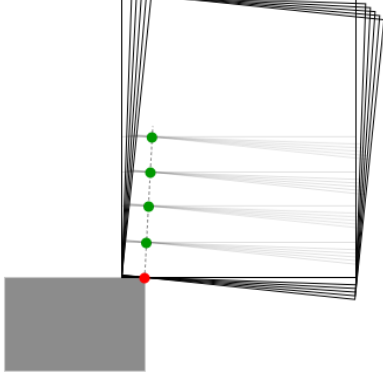


Fig. 6: An object in touch with an environment. The sticking factor enables the iSAM graph to distinguish the red point from the green points.

the external contact to be sticking, only the red dot in Fig.6 is now compatible with the constraints. We incorporate it in the iSAM graph and get a better estimate in the vertical direction. We use a binary factor to impose the sticking constraint:

$$\|F_{tic}(o_{t-1}, o_t, c_{t-1}, c_t)\|_{\Sigma_{tic}}^2 := \|((o_{t-1}^{-1}c_{t-1})^{-1}(o_t^{-1}c_t))_{y^c}\|_{\Sigma_{tic}}^2, \quad (7)$$

where the subscript y^c is the direction on the object's bottom surface perpendicular to the contact line.

Stationary factor (F_{stat}): We assume contact configuration does not change during the motion and the contact line is stationary. This is incorporated by using a binary factor between consecutive timesteps:

$$\|F_{stat}(c_{t-1}, c_t)\|_{\Sigma_{stat}}^2 := \|(c_{t-1}^{-1}c_t)_{y^c, z^c, R_{y^c}, R_{z^c}}\|_{\Sigma_{stat}}^2 \quad (8)$$

B. Active tactile feedback Controller

Fig.5 shows the behavior graph of the active tactile feedback controller. It comprises a push-down phase where the robot moves down until detecting contact, and an active exploration phase where the robot tries to rock and pivot the object about the external contact. During the push-down phase, it executes a proportional control on the gripper-object relative pose estimated by the tactile module:

$$v_z^g = -K_{p,z}(\Delta z_d^g - \Delta z^g) \quad (\text{vertical}) \quad (9)$$

$$\omega_x^g = -K_{p,\phi}(\Delta \phi_d^g - \Delta \phi^g) \quad (\text{roll}) \quad (10)$$

$$\omega_y^g = -K_{p,\theta}(\Delta \theta_d^g - \Delta \theta^g) \quad (\text{pitch}), \quad (11)$$

where $[\omega_x^g, \omega_y^g, \omega_z^g, v_x^g, v_y^g, v_z^g]^T = [\omega^g, v^g]^T$ is the body twist of the gripper frame and the Δ 's are the relative displacement from when the object was not in contact with the environment. The subscript d is for the desired relative displacement. Δz_d^g is set to a non-zero value to ensure the object contacts the environment with sufficient normal force. $\Delta \phi_d^g$ and $\Delta \theta_d^g$ are set to zero.

If the object does not tilt enough so the iSAM graph fails to estimate a contact line with enough confidence, it enters the rocking phase. In the rocking phase, the robot follows a cone-like trajectory by setting the desired relative displacement as below:

$$(\Delta \phi_d^g, \Delta \theta_d^g)(t) = \Delta \phi_0^g (\cos \omega t, \sin \omega t)$$

If the iSAM graph fails to find a contact line even after the rocking, the controller stops and the estimator returns a failure signal.

If the iSAM graph succeeds in estimating an extrinsic contact line either in push-down or rocking, the controller enters the pivoting phase to help the iSAM graph to get more accurate estimate. The controller tries to pivot the object around the extrinsic contact line while avoiding slipping and maintaining a constant tactile deformation. It is assumed that the tactile deformation will remain constant during the pivoting if the object pivots without slipping and also maintaining a constant contact force. Proportional control is used to maintain the deformation as constant as possible:

$$\omega^g = \pm \omega_0 \hat{x}^{gc} - K_{p,\beta}(\Delta \beta_d^g - \Delta \beta^g) \hat{y}^{gc}, \quad (12)$$

$$v^g = p^{gc} \times \omega^g - K_{p,\alpha}(\Delta \alpha_d^g - \Delta \alpha^g) \hat{y}^{gc} - K_{p,z}(\Delta z_d^g - \Delta z^g) \hat{z}^{gc}, \quad (13)$$

where \hat{x}^{gc} and \hat{y}^{gc} are the \hat{x}^c and \hat{y}^c in the gripper coordinate. $\Delta \alpha^g$ and $\Delta \beta^g$ are the components of the relative rotation change in the \hat{x}^c and \hat{y}^c direction. ω_0 is the rotational speed of the pivoting. p^{gc} is the origin of the contact line from the gripper coordinate. The desired relative displacement (Δ_d) is updated to a current relative displacement whenever the pivoting direction changes. The first terms of Eq.12 and Eq.13 rotate the gripper around the current contact line estimate and alters direction ($+\omega_0$ and $-\omega_0$) as it pivots the object back and forth. The second term of Eq.12 and the third term of Eq.13 ensure the object is being pushed down while maintaining the same line contact. The second term of Eq.13 translates the gripper to the direction it reduces slipping.

A key idea in the above method is the synergistic interaction between the controller and the estimator. A better contact line estimation helps the controller to pivot the object with less slipping. On the other hand, a better pivoting around a consistent axis helps the estimator to get a more accurate contact line estimate.

C. RL Policy

The RL policy takes the estimated extrinsic contact line from the estimation graph as the input and computes the SE(2) pose correction for the next insertion attempt (Fig.2d). Since the input to the policy is a low dimensional representation (a single contact line), it is computationally trivial to simulate the policy; given two random shape polygons, each representing the object and the hole, and an SE(2) misalignment between the two, it is easy to find a contact line that the object can pivot around as can be seen in Fig.2c(right). Further details are discussed in Section IV.

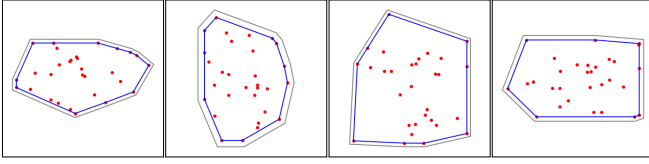


Fig. 7: Random polygonal object-holes

IV. EXPERIMENTAL DETAILS

A. Experimental Setup

Fig. 1 shows the experimental setup. We use a 6-DoF ABB 120 robot arm and a WSG-50 parallel jaw gripper. GelSlim 3.0 [5] sensors are mounted on each side of the jaw gripper. Four types of 3-D printed testing objects are used on seven types of holes and one single wall environment. The average width of the objects is 35mm and the clearance between the objects and the holes is 2.25mm. The top view of each object-hole pair is shown in Table II.

B. Tactile Module Training

The tactile module is trained with supervised learning to estimate the gripper-object relative displacement. It takes a pair of reference tactile images from each side of the sensors at one time and a pair of query tactile images at another time then computes the relative displacement change between the two times. We fix the four objects on the ground with C-clamps then grasp them with random pose and force. Then we randomly wiggle the gripper with Ornstein-Uhlenbeck process noise [28] to collect a training sequence of tactile images. The wiggling motion is clipped with a max limit of (0.25mm, 0.5mm, 0.5mm, 1.2°, 0.6°, 0.2°) in the (x, y, z, roll, pitch, yaw) direction. We regrasp the object after every 10 seconds of the wiggling sequence. 100 sequences for each object are collected and combined in one large training set. The trained tactile module estimates the relative displacement in the (y, z, roll, pitch, yaw) direction with reasonable accuracy: RMSE of (0.07mm, 0.06mm, 0.2°, 0.1°, 0.05°). However, it showed less accuracy in the x direction, the direction perpendicular to the sensor surface: RMSE of 0.12mm. This is expected since it is the direction where the finger gel skin affords less deformation.

C. Active Extrinsic Contact Sensing Experiment

Before testing the entire framework in the insertion task, we decouple only the active extrinsic contact sensing part and test the accuracy of the estimation on the single wall environment. For every grasp, we randomize the grasping height and force. We also vary the horizontal translation and horizontal rotation misalignment between the object and the wall. We say the misalignment is zero when the wall's edge and the object's x-axis match when seen from the top view. Translational error is uniformly sampled from $-12 \sim 12$ mm and rotational error is sampled from $-90^\circ \sim 90^\circ$.

We compare the performance with some ablation models: 'w/o Sticking Factor', 'w/o Deformation Factor', 'w/o Deformation Factor and w/o Pivoting Motion', 'w/o Pivoting Motion', 'w/o Active (rocking & pivoting) Motion', and 'w/o Control'. Note that 'w/o Deformation Factor' means that we

do not incorporate deformation information into the iSAM graph but we still use it as the feedback signal. 'w/o Control' means that there is no feedback so the gripper pushes down with no tilting and the contact line estimation will only rely on the passive compliance of the GelSlim, as in the case of the earlier work that studied extrinsic contact sensing [16].

D. RL Policy Training

RL Policy Training is done fully in simulation. In every episode, to make the policy generalizable to various shapes, we randomize the object polygon by randomly scattering points and drawing their convex hull (blue polygon in Fig. 7). An offset polygon with 2.25mm clearance is used as the hole polygon (black polygon in Fig. 7). The initial misalignment is sampled from $\pm(12\text{mm}, 12\text{mm}, 15^\circ)$. The simulator takes the object-hole polygon and the misalignment as input. Small Gaussian noise (0.2mm, 0.4°) is added to the misalignment to make the policy more robust. The simulator then computes a valid contact line, if one exists, then a Gaussian noise (4mm, 4°) is added to it and returned as an output. If the object polygon intersects with the hole polygon but there is no valid contact line, the simulator returns no line. Lastly, if the object polygon lies inside the hole polygon without intersecting, the simulator returns an insertion success signal.

As a training algorithm, we use twin delayed deep deterministic policy gradient (TD3 [29]) with a recurrent actor. We formulate the task as a partially observed Markov decision process (POMDP). The observation is the estimated contact line and the side in which the object tilts around the contact line. The action is the SE(2) robot displacement from the initial pose. We use the same reward function as in [27]:

$$R_t = e_{t-1} - e_t - P + \chi R_s, \quad (14)$$

where $(e_{t-1} - e_t)$ is a decrease in misalignment from the previous step, P is a small constant penalty term, R_s is a success reward, and χ is the success signal (1 if inserted, 0 otherwise). The maximum sequence length for each episode is set to 15. We train the policy for 15,000 episodes, which takes approximately 15 minutes on GeForce RTX 2080, while it is equivalent to about 1,000 hours of uninterrupted robot experiments.

To deal with partial observability, we use a long short-term memory (LSTM, [30]) for the actor network. It takes the observation and the previous action as the input and outputs the next action. For the critic, we use a multi-layer perceptron (MLP). We directly feed the ground truth misalignment, instead of the partial observation, to the critic. The critic takes the ground truth misalignment and the next action as input and outputs the Q value estimate.

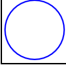
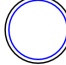
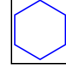
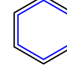

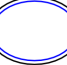

E. Insertion Experiment

We test the entire framework (Contact Sensing + RL Insertion) with the real test objects and holes. For every episode, we vary grasping height and force. Initial misalignment is sampled from $\pm(12\text{mm}, 12\text{mm}, 15^\circ)$. We evaluate the success rate and the average attempt number. The performance is compared with the same ablation models as in Section IV-C.

TABLE I: Accuracy and average error of the active extrinsic contact sensing

	Accuracy (%)		Average Error		
	Easy	Difficult	Horizontal Translation (mm)	Horizontal Rotation (deg)	Vertical Translation (mm)
Active iSAM	95	76	1.80	5.40	3.31
w/o Sticking Factor	91	79	2.13	5.00	11.2
w/o Deformation Factor	92	74	1.74	5.81	3.08
w/o Deformation Factor and w/o Pivoting Motion	79	55	2.58	6.96	5.50
w/o Pivoting Motion	90	75	2.97	6.57	6.50
w/o Active Motion (rocking & pivoting)	88	34	2.37	6.89	5.36
w/o Control (straight push-down)	28	14	3.70	13.1	5.73

TABLE II: Success Rate and average number of insertion attempts (in parentheses) for various object-hole pairs.

Object (blue) & Hole (black) Shape							
Active iSAM-RL	100% (1.94)	97% (1.98)	99% (2.40)	100% (2.94)	95% (2.61)	95% (3.04)	97% (4.13)
w/o Sticking Factor	100% (1.92)	100% (2.02)	100% (2.82)	100% (2.70)	96% (3.15)	94% (2.47)	94% (3.64)
w/o Deformation Factor	100% (2.50)	94% (2.32)	98% (2.75)	96% (3.25)	92% (2.83)	96% (2.77)	90% (4.76)
w/o Active Motion	96% (2.15)	94% (2.00)	94% (2.70)	94% (3.51)	90% (3.02)	90% (2.73)	86% (4.77)
w/o Control (straight push-down)	46% (4.17)	46% (5.87)	54% (5.52)	34% (4.82)	58% (4.62)	54% (4.19)	30% (5.60)
RL-end2end (Dong [27])	97% (2.96)	-	97% (3.83)	-	98% (2.34)	-	90% (5.42)
SL-end2end (Dong [26])	85% (3.04)	-	70% (3.34)	-	94% (2.60)	-	15% (3.83)

V. RESULTS

A. Active Extrinsic Contact Sensing Experiment

Table I shows the performance of the proposed method and ablation models in the contact sensing experiment on the wall environment, in 100 trials per object. Accuracy is the rate at which the method estimates the contact line with horizontal translation error less than 7mm and rotational error less than 25° . We show accuracy separately for easy cases and difficult cases. The easy cases are when the gripper center seen from the top view lies on the same side of the tilting side and the horizontal distance between the gripper center and the contact line is larger than 5mm.

Our method showed an accuracy of 95% for easy cases and 76% for difficult cases. As explained in Section III-A, a model without the sticking factor showed reasonable performance in the horizontal direction but the vertical error was about 3.4 times larger than the original version.

‘w/o Deformation Factor’ shows a similar performance as the original. This is because the deformation is kept almost constant during the pivoting motion so the deformation factor becomes less important. However, ‘w/o Deformation Factor and w/o Pivoting Motion’ showed poorer performance than ‘w/o Pivoting Motion’ because the deformation fluctuates significantly during the push-down and the rocking motion.

For ‘w/o Active Motion’, the accuracy drops, especially for the difficult cases. In difficult cases, the gripper center seen from the top view lies on the wall so it is difficult to

tilt with only the push-down motion. In such a case, the active rocking motion is necessary to get a significant tilting angle and estimate a contact line. ‘w/o Control’ shows the poorest performance meaning that the GelSlim compliance solely does not provide sufficient information to estimate a contact line.

B. Insertion Experiments

Table II shows the insertion performance of the proposed method, ablation models, and previous work [26], [27], in 100 episodes per case. The performance is evaluated in success rate and in the average number attempt until the insertion succeeds. Note that [26], [27] used the shown cases as training cases, while ours used them as testing cases. Also, they used smaller misalignment (6mm, 6mm, 10°) than ours (12mm, 12mm, 15°).

Our method shown a higher than 95% success rate in all the test cases. Especially for the rectangle object-hole, the success rate was 7% higher and the attempt number was 24% lower than the previous work.

‘w/o Sticking Factor’ shows a similar performance as the original since it has the similar contact line estimation performance in the horizontal direction as seen in Section V-A. The performance decreases slightly for ‘w/o Deformation Factor’. ‘w/o Active Motion’ shows poorer performance, especially for the rectangle object-hole case.

VI. CONCLUSION AND FUTURE WORK

We propose a framework for active extrinsic contact sensing and applied it to an insertion policy by using the estimated contact line as an input to an insertion policy trained in simulation with RL. The iSAM-based estimation model and the active tactile feedback controller work collaboratively to localize the contact line between a grasped object and an environment. We then formulate the insertion task as an RL problem where the input is the series of estimated contacts with the hole. This enabled us to train the RL agent completely in simulation and ease the burden of collecting training data with real experiments. In future work, we would like to extend this framework to more general manipulation scenarios: point contacts, non-stationary contacts, and non-flat object/environment surfaces.

REFERENCES

- [1] R. D. Howe, "Tactile sensing and control of robotic manipulation," *Advanced Robotics*, vol. 8, no. 3, pp. 245–261, 1993.
- [2] A. Rodriguez, "The unstable queen: Uncertainty, mechanics, and tactile feedback," *Science Robotics*, vol. 6, no. 54, 2021.
- [3] W. S. Newman, Y. Zhao, and Y.-H. Pao, "Interpretation of force and moment signals for compliant peg-in-hole assembly," in *Proceedings 2001 ICRA. IEEE International Conference on Robotics and Automation (Cat. No. 01CH37164)*, vol. 1. IEEE, 2001, pp. 571–576.
- [4] M. Kaess, A. Ranganathan, and F. Dellaert, "isam: Incremental smoothing and mapping," *IEEE Transactions on Robotics*, vol. 24, no. 6, pp. 1365–1378, 2008.
- [5] I. Taylor, S. Dong, and A. Rodriguez, "Gelslim 3.0: High-resolution measurement of shape, force and slip in a compact tactile-sensing finger," *arXiv preprint arXiv:2103.12269*, 2021.
- [6] A. Bicchi, J. K. Salisbury, and D. L. Brock, "Contact sensing from force measurements," *The International Journal of Robotics Research*, vol. 12, no. 3, pp. 249–262, 1993.
- [7] K.-T. Yu and A. Rodriguez, "Realtime state estimation with tactile and visual sensing. application to planar manipulation," in *2018 IEEE International Conference on Robotics and Automation (ICRA)*. IEEE, 2018, pp. 7778–7785.
- [8] —, "Realtime state estimation with tactile and visual sensing for inserting a suction-held object," in *2018 IEEE/RSJ International Conference on Intelligent Robots and Systems (IROS)*. IEEE, 2018, pp. 1628–1635.
- [9] W. Yuan, S. Dong, and E. H. Adelson, "Gelsight: High-resolution robot tactile sensors for estimating geometry and force," *Sensors*, vol. 17, no. 12, p. 2762, 2017.
- [10] E. Donlon, S. Dong, M. Liu, J. Li, E. Adelson, and A. Rodriguez, "Gelslim: A high-resolution, compact, robust, and calibrated tactile-sensing finger," in *2018 IEEE/RSJ International Conference on Intelligent Robots and Systems (IROS)*. IEEE, 2018, pp. 1927–1934.
- [11] M. Bauza, O. Canal, and A. Rodriguez, "Tactile mapping and localization from high-resolution tactile imprints," in *2019 International Conference on Robotics and Automation (ICRA)*. IEEE, 2019, pp. 3811–3817.
- [12] M. Bauza, E. Valls, B. Lim, T. Sechopoulos, and A. Rodriguez, "Tactile object pose estimation from the first touch with geometric contact rendering," in *Conference on Robot Learning (CoRL)*. IEEE, 2020.
- [13] D. Ma, E. Donlon, S. Dong, and A. Rodriguez, "Dense tactile force estimation using gelslim and inverse fem," in *2019 International Conference on Robotics and Automation (ICRA)*. IEEE, 2019, pp. 5418–5424.
- [14] P. Sodhi, M. Kaess, M. Mukadam, and S. Anderson, "Learning tactile models for factor graph-based estimation," in *2021 International Conference on Robotics and Automation (ICRA)*. IEEE, 2021.
- [15] M. Lambeta, P.-W. Chou, S. Tian, B. Yang, B. Maloon, V. R. Most, D. Stroud, R. Santos, A. Byagowi, G. Kammerer *et al.*, "Digit: A novel design for a low-cost compact high-resolution tactile sensor with application to in-hand manipulation," *IEEE Robotics and Automation Letters*, vol. 5, no. 3, pp. 3838–3845, 2020.
- [16] D. Ma, S. Dong, and A. Rodriguez, "Extrinsic contact sensing with relative-motion tracking from distributed tactile measurements," in *2021 International Conference on Robotics and Automation (ICRA)*. IEEE, 2021.
- [17] K. S. Arun, T. S. Huang, and S. D. Blostein, "Least-squares fitting of two 3-d point sets," *IEEE Transactions on pattern analysis and machine intelligence*, no. 5, pp. 698–700, 1987.
- [18] S. Dong, D. Ma, E. Donlon, and A. Rodriguez, "Maintaining grasps within slipping bounds by monitoring incipient slip," in *2019 International Conference on Robotics and Automation (ICRA)*. IEEE, 2019, pp. 3818–3824.
- [19] F. R. Hogan, J. Ballester, S. Dong, and A. Rodriguez, "Tactile dexterity: Manipulation primitives with tactile feedback," in *2020 IEEE international conference on robotics and automation (ICRA)*. IEEE, 2020, pp. 8863–8869.
- [20] Y. She, S. Wang, S. Dong, N. Sunil, A. Rodriguez, and E. Adelson, "Cable manipulation with a tactile-reactive gripper," *The International Journal of Robotics Research*, 2021.
- [21] D. E. Whitney, "Quasi-static assembly of compliantly supported rigid parts," *Journal of Dynamic Systems, Measurement, and Control*, vol. 104, no. 1, pp. 65–77, 1982.
- [22] M. E. Came, T. Lozano-Pérez, and W. P. Seering, "Assembly strategies for chamferless parts," in *Proceedings of the IEEE International Conference on Robotics and Automation*, 1989, pp. 472–477.
- [23] H. Bruyninckx, S. Dutre, and J. De Schutter, "Peg-on-hole: a model based solution to peg and hole alignment," in *Proceedings of 1995 IEEE International Conference on Robotics and Automation*, vol. 2. IEEE, 1995, pp. 1919–1924.
- [24] T. Inoue, G. De Magistris, A. Munawar, T. Yokoya, and R. Tachibana, "Deep reinforcement learning for high precision assembly tasks," in *2017 IEEE/RSJ International Conference on Intelligent Robots and Systems (IROS)*. IEEE, 2017, pp. 819–825.
- [25] M. A. Lee, Y. Zhu, P. Zachares, M. Tan, K. Srinivasan, S. Savarese, L. Fei-Fei, A. Garg, and J. Bohg, "Making sense of vision and touch: Learning multimodal representations for contact-rich tasks," *IEEE Transactions on Robotics*, vol. 36, no. 3, pp. 582–596, 2020.
- [26] S. Dong and A. Rodriguez, "Tactile-based insertion for dense box-packing," in *2019 IEEE/RSJ International Conference on Intelligent Robots and Systems (IROS)*. IEEE, 2019, pp. 7953–7960.
- [27] S. Dong, D. K. Jha, D. Romeres, S. Kim, D. Nikovski, and A. Rodriguez, "Tactile-RL for insertion: Generalization to objects of unknown geometry," in *2021 International Conference on Robotics and Automation (ICRA)*. IEEE, 2021.
- [28] G. E. Uhlenbeck and L. S. Ornstein, "On the theory of the brownian motion," *Phys. Rev.*, vol. 36, pp. 823–841, Sep 1930.
- [29] S. Fujimoto, H. Hoof, and D. Meger, "Addressing function approximation error in actor-critic methods," in *International Conference on Machine Learning*. PMLR, 2018, pp. 1587–1596.
- [30] S. Hochreiter and J. Schmidhuber, "Long short-term memory," *Neural Computation*, vol. 9, no. 8, pp. 1735–1780, 1997.